# Optics Letters

# Non-iterative multifold strip segmentation phase method for six-dimensional optical field modulation: supplement

YUEQIANG ZHU,[1] WEI ZHAO,[1,2] CHEN ZHANG,[1] KAIGE WANG,[1,3] AND JINTAO BAI[1]

[1]*State Key Laboratory of Photon-Technology in Western China Energy, International Collaborative Center on Photoelectric Technology and Nano Functional Materials, Institute of Photonics & Photon Technology, Northwest University, Xi'an 710127, China*
[2]*e-mail: zwbayern@nwu.edu.cn*
[3]*e-mail: wangkg@nwu.edu.cn*

# Non-iterative multifold strip segmentation phase method for six-dimensional optical field modulation: supplementary material

## Yueqiang Zhu, Wei Zhao*, Chen Zhang, Kaige Wang* and Jintao Bai

[1]State Key Laboratory of Photon-Technology in Western China Energy, International Collaborative Center on Photoelectric Technology and Nano Functional Materials, Institute of Photonics & Photon Technology, Northwest University, Xi'an 710127, China

*Corresponding author: zwbayern@nwu.edu.cn, wangkg@nwu.edu.cn

## S1. Generating multi-focus light field by multifold strip segmentation phase (MSSP) method

MSSP method is schematically described in Fig. S1. As an example shown in Fig. S1(d), to generate a complex light field of two spots (one vortex beam and one Bessel-Gaussian beam) with SLM, we generate a phase pattern using the SSP method ([1]) first. Then, in Fig. S1(b), we again use SSP method to generate the phase map for vortex beam. Finally, as shown in Fig. S1(c), the phase pattern to generate the two-spot light field are assembled. According to the phase pattern of MSSP, a complex light field with one vortex beam and one Bessel-Gaussian beam is generated at the positions $(\Delta x, \Delta y) = (0,2)$ μm and $(0, -2)$ μm respectively.
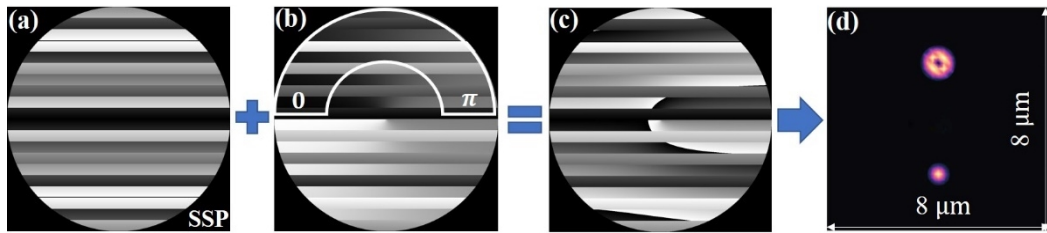


**Fig. S1.** Schematic of generating multi-focus light field by multifold strip segmentation phase (MSSP) method. (a) The phase pattern of strip segmentation phase (SSP) to generate two focal, where $N = 10$, $M = 2$ (b) SSP method to generate phase map of vortex beam with topological charge $l = 1$. Here, $N = 10$, $M = 2$. (c) Phase pattern of MSSP is realized by combining (a) and (b). (d) The corresponding light intensity distribution using (c) from numerical simulation.

## S2. Phase expressions for generating multi-focus light field

**Table. S1** Phase-only expressions about multi-focus light field

| Spot | Phase function | Notes |
|---|---|---|
| Bessel-Gaussian beam | $\phi_1 = k_0 r \tan \alpha_1$ | $k_0 = 2\pi/\lambda$ is the wave number, $r = \sqrt{x'^2 + y'^2}$ is polar coordinate at the back-aperture plane, $\alpha_1$ is the angle of axicon |

| | | lens. |
|---|---|---|
| Perfect vortex beam | $\phi_2 = l\varphi + \eta r$ | $l$ is topological charge, $\varphi \in [0, 2\pi]$ is azimuthal angle of polar coordinates at the back-aperture plane, $\eta$ is the axicon parameter, which could be used to control the diameter of perfect vortex-like beam in the focusing region. $r = \sqrt{x'^2 + y'^2}$ is radial position of polar coordinates at the back-aperture plane. |
| Perfect vortex-like beam | $\phi_3 = l\varphi + \eta r_2$ | $r_2 = \sqrt{x_2{}^2 + y_2{}^2}$ can be obtained by rotating radial position $r$ |
| Spiral focal spot | $\phi_4 = -l_1\text{sign}(y')\arccos(x'/r)$ $-l_2\text{sign}(y')\arccos\left(\dfrac{x'-aR}{\sqrt{(x'-aR)^2}}\right)$ $-l_3\text{sign}(y')\arccos\left(\dfrac{x'-bR}{\sqrt{(x'-bR)^2}}\right)$ | $a$ and $b$ are the translation coefficient along the $x'$ coordinate. $l_1$, $l_2$ and $l_3$ are the topological charges of three spatially shifted vortex beams. sign $(y')$ is a correction for the phase when $y' < 0$, $R$ is the maximum radius of the back aperture. |
| Airy beam | $\phi_5 = (k_x{}^3 + k_y{}^3) - c(k_x{}^2 + k_y{}^2$ | $c$ is the decaying factor to truncate the tail of the infinite Airy beam, and $c \ll 1$. $k_x$ and $k_y$ representing the wave number components in $x$ and $y$ directions respectively. |
| Airy-like beam | $\phi_6 = (k_{x2}{}^3 + k_{y2}{}^3) - c(k_{x2}{}^2 + $ | $c$ is the decaying factor to truncate the tail of the infinite Airy beam, and $c \ll 1$, $k_{x2}$ and $k_{y2}$ can be obtained by rotating $k_x$ and $k_y$. |

## S3. The principle of the six-dimensional optical modulation by phase-only expression

According to the shift theorem of Fourier transform, the focal spot can be translated moved in 3D space as

$$E(x - \Delta x, y - \Delta y, z - \Delta z) = \mathcal{F}^{-1}\{U(\theta,\varphi)P(\theta)E_t(\theta,\varphi)e^{ik_z z}/\cos\theta\} \quad (S1)$$

where $\mathcal{F}^{-1}(\cdot)$ denotes inverse Fourier transform, $P(\theta)$ is the apodization function, $E_t(\theta,\varphi)$ is a transmission field [2], $\theta = \arcsin(r\text{NA}/Rn_t)$ is the converge angle of objective lens, $R$ is the maximum radius of the back aperture plane, $r$ and $\varphi$ are the radial position and azimuthal angle of polar coordinates at the back aperture plane. $n_t = 1.518$ is the medium refractive index behind oil-immersion objective. $U(\theta,\varphi) = \exp^{i(\phi+\phi_x)}$ is a phase modulation function on the back aperture of an aberration-free objective lens, where $\phi = k_x\Delta x + k_y\Delta y + k_z\Delta z$ (where $\Delta x$, $\Delta y$ and $\Delta z$ are the displacements of the focal spot in $x$, $y$ and $z$ directions on the focal region of the objective lens) is the phase-only analytical equation for controlling the 3D position. Let $x'$ and $y'$ be the Cartesian coordinates in the back aperture of objective lens, it is easily found $x' = r\cos\varphi$ and $y' = r\sin\varphi$. Then, considering $\sin\theta = r\text{NA}/Rn_t$, the spatial

frequency $k_x$, $k_y$ and $k_z$ can be alternately expressed as $k_x = 2\pi x'\text{NA}/Rn_t\lambda$, $k_y = 2\pi y'\text{NA}/Rn_t\lambda$ and $k_z = 2\pi\sqrt{1 - (x'^2 + y'^2)/\left(Rn_t/\text{NA}\right)^2}/\lambda$. Finally, after substituting $k_x$, $k_y$ and $k_z$ into $\phi$, we have

$$\phi(x',y') = \frac{2\pi}{\lambda} \times \left[\frac{NA}{Rn_t}(x'\varDelta x + y'\varDelta y) + \varDelta z\sqrt{1 - \frac{x'^2 + y'^2}{\left(Rn_t/\text{NA}\right)^2}}\right] \tag{S2}$$

In addition, $\phi_x$ is any phase distribution designed, e.g., controlling the 3D rotational motions of the beam focuses, which can be realized by introducing a transfer matrix (Eq. S3) $\boldsymbol{M}$ into $\phi_x$. $\boldsymbol{M}$ can be expressed as

$$\boldsymbol{M} = \begin{bmatrix} \cos\theta_3\cos\theta_2 & \cos\theta_3\sin\theta_2\sin\theta_1 - \sin\theta_3\cos\theta_1 & \cos\theta_3\sin\theta_2\cos\theta_1 + \sin\theta_3\sin\theta_1 \\ \sin\theta_3\cos\theta_2 & \sin\theta_3\sin\theta_2\sin\theta_1 + \cos\theta_3\cos\theta_1 & \sin\theta_3\sin\theta_2\cos\theta_1 - \cos\theta_3\sin\theta_1 \\ -\sin\theta_2 & \cos\theta_2\sin\theta_1 & \cos\theta_2\cos\theta_1 \end{bmatrix}$$

$$= \begin{bmatrix} \boldsymbol{M}(1) \\ \boldsymbol{M}(2) \\ \boldsymbol{M}(3) \end{bmatrix} \tag{S3}$$

where $\boldsymbol{M}(1)$, $\boldsymbol{M}(2)$ and $\boldsymbol{M}(3)$ are the first, second and third row vectors of $\boldsymbol{M}$ respectively, $\theta_1,\theta_2,\theta_3 \in [0, 2\pi]$ are the rotation angles in $x-$, $y-$ and $z-$directions, respectively. For instance, to rotate a perfect vortex beam, we have

$$\phi_x = l\varphi + \eta\sqrt{\left\{\boldsymbol{M}(1)\cdot\begin{bmatrix} x' \\ y' \\ z \end{bmatrix}\right\}^2 + \left\{\boldsymbol{M}(2)\cdot\begin{bmatrix} x' \\ y' \\ z \end{bmatrix}\right\}^2} = l\varphi + \eta\sqrt{x_2^2 + y_2^2} \tag{S4}$$

The coordinate $z$ is the beam propagation direction, $x_2 = \boldsymbol{M}(1)\cdot\begin{bmatrix} x' \\ y' \\ z \end{bmatrix}$ and $y_2 = \boldsymbol{M}(2)\cdot\begin{bmatrix} x' \\ y' \\ z \end{bmatrix}$ are the coordinates after rotation. Based on this point, three-dimensional rotations have been successfully achieved. Therefore, to realize six-dimensional optical modulation of perfect vortex beam, we have

$$U(\theta,\varphi) = e^{i(\phi+\phi_x)}$$

$$= e^{i\left\{\frac{2\pi}{\lambda}\left[\frac{NA}{Rn_t}(x'\varDelta x + y'\varDelta y) + \varDelta z\sqrt{1 - \frac{x'^2 + y'^2}{\left(Rn_t/\text{NA}\right)^2}}\right] + l\varphi + \eta\sqrt{x_2^2 + y_2^2}\right\}} \tag{S5}$$

the modulation on 3D translational positions and 3D rotations can be simultaneously realized. This method can be applied for any beam in multi-focus light field, including Airy-like beam, Bessel-Gaussian beam, perfect vortex beam and etc.


## S4. Experimental setup and procedure for generating multi-focus light field

To further illustrate the feasibility of our method in practical applications with high-NA objective lens, an experimental system developed based on an inverted fluorescence microscope has been built to generate multi-focus fluorescent light field, as shown in Fig. S2(a). A 639 nm continuous-wave laser (MW-RL-639/400 mW, CNI) is used as a light source in the fluorescent imaging experiment. The beam is first modulated by a spatial pinhole filter (SPF) (OptoSigma, SFB-16DM) and lenses (L) to for better

beam quality and collimation. The redundant diffraction ring is filtered by iris diaphragm (ID1). A polarizer (P) is applied to generate a linearly polarized beam, of which the polarization direction is parallel to the working direction of the liquid crystal plate of the SLM (LETO, HOLOEYE Photonics AG, Germany, PLUTO-NIR-011, 420 nm~1100 nm). Then, the beam passes through a beam splitter (THORLABS, BS 400 nm~800 nm) and reaches the SLM. A second iris diaphragm (ID2) is used to adjust the diameter of the beam at SLM. The beam after modulation further passes a quarter-wave plate (THORLABS), and imported into an inverted fluorescence microscope (NIB900, NEXCOPE, China) by reflective mirrors (R). A dichroic mirror (SEMROCK, Di01-R488/543/635, 405 nm HR, 639 nm HR) and a bandpass filter (CHROMA, ZET488/640m) is used in the microscope. Therefore, the 639 nm beam is reflected by the dichroic mirror and focused with a high-NA objective lens (Leica, PL Apo 63X, NA 1.4). The fluorescent spots pass through the same dichroic mirror and the bandpass filter sequentially, and are finally captured by a SCMOS (PCO AG, Kelheim, Germany, PCO. edge 4.2m) camera.

In the experiment, CY5 (Bridgen) was used as fluorescent dye. It has an excitation peak at 651 nm and emits fluorescence at 670 nm (see Fig. S2(b)). During sample preparation, CY5 solid powder is first dissolved by deionized water (DI) for a concentration of 1.25 µM. Then, we mixed the dye solution with refractive index matching liquid Mowiol® 4-88 (Sigma-Aldrich) under a ratio of 3:2. The Mowiol® 4-88 liquid has a refractive index of 1.518 which is consistent with that of the cover slip and immersion oil. Thus, the difference of refractive indices between solution and coverslip can be significantly reduced, accompanied by the smaller influence of aberration caused by refractive index mismatch [3]. During measurement, several drops of the mixed solution were placed on a coverslip and evaporated. After the droplets are dried, a thin film can be formed on the coverslip. Accompanied with z-directional scanning, the images of fluorescent spots on different z positions were captured. Finally, the 3D distribution of fluorescence (e.g. in Fig. 3) can be produced.
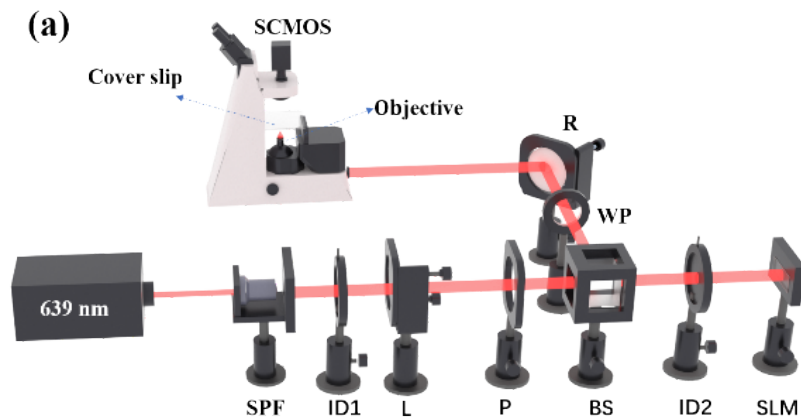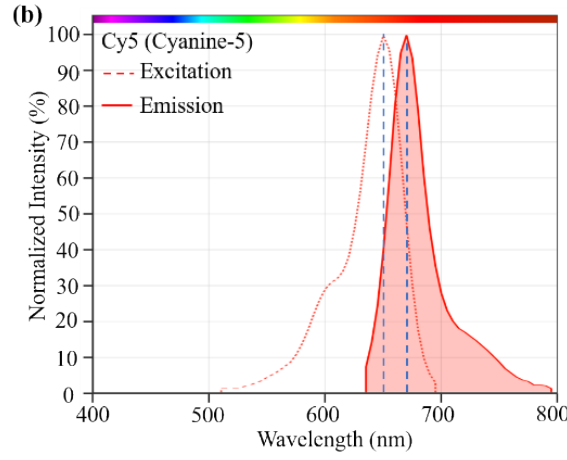
**Fig. S2** (a) Schematic of the optical system for generating multifocal spots; SPF is spatial pinhole filters; ID1 and ID2 are iris diaphragm; L is a collimation lens; P is a polarizer; BS is a beam splitter; SLM is a liquid-crystal-on-silicon spatial light modulator; WP is a quarter-wave plate; R is reflective mirrors. (b) Excitation and emission spectra of Cy5 fluorescent dyes (the data is from Bridgen).

## S5. The method of eliminating the influence zero-order light
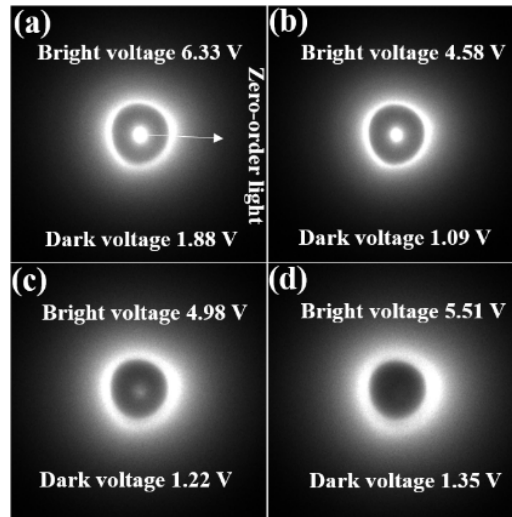


**Fig. S3.** Fluorescent image results of perfect vortex beams ($l = 5$, $\eta = 12$ μm) to reveal the influence of Bright and Dark voltage parameters of SLM on zero-order light. (a) Bright voltage is 6.33 V and Dark voltage is 1.88 V. (b) Bright voltage is 4.58 V and Dark voltage is 1.09V. (c) Bright voltage is 4.98 V and Dark voltage is 1.22 V. (d) Bright voltage is 5.51 V and Dark voltage 1.35 V.

In the experiment, to inhibit the influence of zero-order light due to spatial light modulator pixilation [4], a method of adjusting the Bright and Dark voltage parameters of SLM is applied. As shown in Fig. S3 are the experimental results of adjusting the zero-order light by changing the voltage. Here, a perfect vortex beam ($l = 5$, $\eta = 12$ μm) is used. It can be seen from Fig. S3(a-i) that the influence of zero-order light

gradually decreases or even disappears by gradually changing the value of Bright and Dark voltage. Interestingly, these Bright and Dark voltage values are all departure from the official values (6.33V and 1.88V) at this wavelength (see Fig. S3(A)). However, the actual Bright and Dark voltages for eliminating zeroth-order light rely on the type of SLM and wavelength of incident beam, and should be experimentally determined. Therefore, this method is very valuable for a broad application, e.g., laser fabrication, laser imaging, optical storage and etc.

## S6. Detailed parameters of optical modulation used in figures
## (1) Parameters of optical modulation used in Fig. 2

**Table. S2** Parameters of optical modulation used in Fig. 2. Length units in μm.

| Fig. 2(a) | Fig. 2(b) | Fig. 2(c) | Fig. 2(d) | Fig. 2(e) | Fig. 2(f) |
|---|---|---|---|---|---|
| One Bessel-Gaussian beam | One Bessel-Gaussian beam | Three Airy-like beams | One perfect vortex beam | One perfect vortex beam | One spiral spot |
| $(\Delta x, \Delta y)=$ (0,0.3) $\alpha_1 = \pi/4$ | $(\Delta x, \Delta y)=(0,0)$ | $(\Delta x, \Delta y)=$ $(0, -1)$ $(\Delta x, \Delta y)=(0,1)$ $(\Delta x, \Delta y)=(0,0)$ $\theta_1 = \pi/2$ | $(\Delta x, \Delta y)=$ (0,0) $l = 1, \ \eta = 8$ | $(\Delta x, \Delta y)=$ (0,0) $l = 1, \ \eta = 14$ | $(\Delta x, \Delta y)=$ (0,0) a=0.25, b=0.65, $l_1 = 4, \ l_2 = 1, \ l_3 = 1,$ $\theta_1 = -\pi/4$ |
| | One spiral spot | | One perfect vortex beam | | |
| One perfect vortex beam | $(\Delta x, \Delta y)=$ $(-2, -2)$ $a = 0.25,$ $b = 0.65$ $l_1 = 4, \ l_2 = 1,$ $l_3 = 1$ | | $(\Delta x, \Delta y)=$ (0,0) $l = 5, \ \eta = 6$ | | |
| $(\Delta x, \Delta y)=$ $(0, -0.3)$ $l = 1$ | One perfect vortex beam | One perfect vortex beam | One Bessel-Gaussian beam | One Airy beam | One perfect vortex-like beam |
| | $(\Delta x, \Delta y)=(2,2)$ $l = 2, \eta = 2$ | $(\Delta x, \Delta y)=(0,0)$ $l = 1, \eta = 12$ | $(\Delta x, \Delta y)=$ (0,0) $\alpha_1 = \pi/4$ | $(\Delta x, \Delta y)=$ (0,0) $c = 0.51$ | $(\Delta x, \Delta y)=$ (0,0) $\theta_1 = \pi/4$ |

In visualization 1 (uploaded as a single file), Fig. 2(e) and perfect vortex-like beam can be dynamically rotated by dynamically changing the phase pattern on SLM. The corresponding light intensity distribution are shown in the second row of Fig. 2. The corresponding fluorescent intensity distributions recorded by SCMOS camera in an inverted microscopy are shown in the third row of Fig. 2.

## (2) Parameters of optical modulation used in Fig. 3
**Table. S3** Parameters of optical modulation used in Fig. 3. Length units in μm.

| Perfect vortex | $\Delta x$ | $\Delta y$ | $\Delta z$ | $\theta_1$ | $l$ | $\eta$ |
|---|---|---|---|---|---|---|
| beam (from the top plane to the | 0 | 3 | 0 | 0 | 1 | 2 |
| | | | 0.3 | 0 | 1 | 4 |

| | $\Delta x$ | $\Delta y$ | $\Delta z$ | $\theta_1$ | | |
|---|---|---|---|---|---|---|
| bottom plane) | | | 0.6 | 0 | 1 | 6 |
| | | | 0.9 | 0 | 1 | 8 |
| Airy-like beam (from the top plane to the bottom plane) | $\Delta x$ | $\Delta y$ | $\Delta z$ | $\theta_1$ | $c$ | |
| | -3 | 0 | 0 | $3\pi/4$ | 0.22 | |
| | | | 0.3 | $\pi/4$ | 0.22 | |
| | | | 0.6 | 0 | 0.22 | |
| | | | 0.9 | $7\pi/4$ | 0.22 | |
| Perfect vortex-like beam (from the top plane to the bottom plane) | $\Delta x$ | $\Delta y$ | $\Delta z$ | $\theta_1$ | $l$ | $\eta$ |
| | 0 | -3 | 0 | $\pi/4$ | 1 | 10 |
| | | | 0.3 | $3\pi/4$ | 1 | 10 |
| | | | 0.6 | $\pi/4$ | 1 | 10 |
| | | | 0.9 | $3\pi/4$ | 1 | 10 |
| spiral focal spot (from the top plane to the bottom plane) | $\Delta x$ | $\Delta y$ | $\Delta z$ | $\theta_1$ | $(a,b)$ | $(l_1,l_2,l_3)$ |
| | 3 | 0 | 0 | $3\pi/4$ | (0.25,0.65) | (3,1,1) |
| | | | 0.3 | $5\pi/4$ | (0.25,0.65) | (3,1,1) |
| | | | 0.6 | $7\pi/4$ | (0.25,0.65) | (5,1,1) |
| | | | 0.9 | $\pi/4$ | (0.25,0.65) | (5,1,1) |
| Bessel-Gaussian beam (from the top plane to the bottom plane) | $\Delta x$ | $\Delta y$ | $\Delta z$ | $\theta_1$ | $\alpha_1$ | |
| | 0 | 0 | 0 | 0 | $\pi/4$ | |
| | | | 0.3 | 0 | $\pi/4$ | |
| | | | 0.6 | 0 | $\pi/4$ | |

| | | 0.9 | 0 | $\pi/4$ |
|---|---|---|---|---|

## (3) Parameters of optical modulation used in Fig. 4

**Table. S4** Parameters of optical modulation used in Fig. 4. Length units in μm.

| Beam 1 | $\Delta x$ | $\Delta y$ | $\Delta z$ | $\theta_1$ | $\theta_2$ | $\theta_3$ | $c$ | |
|---|---|---|---|---|---|---|---|---|
| | 3 | 3 | 1 | $\pi/4$ | $\pi/4$ | $\pi/4$ | 0.42 | |
| Beam 2 | $\Delta x$ | $\Delta y$ | $\Delta z$ | $\theta_1$ | $\theta_2$ | $\theta_3$ | $l$ | $\eta$ |
| | 3 | -3 | 0 | 0 | $\pi/4$ | $\pi/4$ | 2 | 4 |
| Beam 3 | $\Delta x$ | $\Delta y$ | $\Delta z$ | $\theta_1$ | $\theta_2$ | $\theta_3$ | $\alpha_1$ | |
| | -3 | -3 | -1 | $\pi/4$ | 0 | $\pi/4$ | $\pi/4$ | |
| Beam 4 | $\Delta x$ | $\Delta y$ | $\Delta z$ | $\theta_1$ | $\theta_2$ | $\theta_3$ | $l$ | $\eta$ |
| | -3 | 3 | 0 | $\pi/4$ | 0 | $\pi/4$ | 2 | 4 |

Visualization 2 and 3 (uploaded as a single file) show the dynamical rotation of the 3D structures of the beam.

## S7. Light diffraction efficiency of modulation

The light diffraction efficiency $\beta$ of modulation is defined as [5]

$$\beta = \sum_{m=1}^{M} \iint_{\Omega_m} I_s \mathrm{d}x\mathrm{d}y \Big/ \iint_{\Omega'} I_s \mathrm{d}x\mathrm{d}y \qquad (S6)$$

where $M = 20$ is the number of multifocal spots, $I_s$ represents the light intensity distribution from simulation, $\Omega_m$ is the region of the $m^{\text{th}}$ focal spot, $\Omega'$ denotes the entire illumination. The calculation of the light diffraction efficiency $\beta$ is carried out for the simulation in Fig. 3(d). Fig. 3(d) shows that as the number of $N$ increases, the light diffraction efficiency is clearly increased.

## REFERENCES

1. Y. Zhu, C. Zhang, Y. Gong, W. Zhao, J. Bai, and K. Wang, Optics Express **29**, 8698-8709 (2021).
2. Marcel Leutenegger, Ramachandra Rao, Rainer A. Leitgeb, and T. Lasser, Optics Express **14**, 11277-11291 (2006).
3. Y. Zhu, C. Zhang, W. Zhao, J. Wang, K. Wang, and J. Bai, Journal of Microscopy (2021).
4. S. Ji, L. Yang, Y. Hu, J. Ni, W. Du, J. Li, G. Zhao, D. Wu, and J. Chu, Small **13** (2017).
5. T. Zeng, C. Chang, Z. Chen, H.-T. Wang, and J. Ding, Journal of Optics **20** (2018).